Aeroelastic Mode Control using $\mathcal{H}_2$-optimal Blends for Inputs and Outputs

Manuel Pusch*

German Aerospace Center (DLR), 82234 Wessling, Germany

For flexible aircraft, it is often required to control individual aeroelastic modes which are lightly damped or even unstable. In order to achieve a maximum controller performance, a large number of measurements and control surfaces is required, which in turn complicates controller design. Blending control inputs and measurement outputs, individual aeroelastic modes can be isolated efficiently and hence controlled by a single input single output controller. In this paper, a novel approach is presented for designing $\mathcal{H}_2$-optimal blending vectors for the control of individual aeroelastic modes. An efficient algorithm is derived to jointly compute the interdependent input and output blending vectors, where an explicit mode decoupling can be considered. The effectiveness of the proposed approach is proven by designing a gust load alleviation system for a flexible aircraft with distributed flaps and measurements.

I. Introduction

In order to improve aircraft performance, structural weight reduction and aerodynamically efficient high aspect ratio wings play a key role.[1] This, however, typically leads to a reduced separation between rigid body and flexible modes as well as an increased sensitivity to gust encounters.[2] To counteract these adverse effects, active control can be used by feeding back multiple measurements to available control surfaces. Increasing the number of measurements or multifunctional control surfaces allows improving aircraft performance,[3] but also leads to new challenges in the design and certification of the flight control system.[4]

In general, a reasonable control design requires a thorough modeling of the underlying physical system.[5] For an aeroelastic system, this includes the description of complex effects like the coupling of unsteady aerodynamics with structural dynamics leading to models with a large number of highly coupled states.[6] For the control of the described adverse effects, however, typically only few aeroelastic modes need to be considered while the residual modes should not be affected.

Generalizing the described control problem, the objective is to control few out of a large number of modes by feeding back multiple measurements outputs to multiple control inputs. In order to solve this control problem, observer based methods may be used, where a prior model order reduction is recommended or even necessary for controller synthesis.[5] In the case of a large number of measurements, this can be avoided by blending the measurement signals in a way such that the resulting virtual output represents the response of a single mode. Similarly, a virtual input can be generated which allows an explicit control of a single mode. As a result, single input and single output (SISO) systems are derived which isolate the modes of interest and enable the design of SISO controllers.

In order to achieve the desired mode isolation, appropriate blending vectors need to be designed. As the input and output blending vectors can not be designed independent of each other, an iterative procedure is proposed, for instance, in Ref. 7. In the given algorithm, denoted as "modal isolation and damping for adaptive aeroservoelastic suppression" (MIDAAS), the input and output blending vectors are computed by different methods and directly provide a static gain feedback controller. Another iterative approach is presented in Ref. 8, where the inputs and outputs are blended in order to allow a SISO notch filter design for suppressing individual modes. Apart from this, a SISO controller design may also be enabled by diagonalizing a multiple inputs and multiple outputs (MIMO) system such that individual inputs allow to control individual

*Research Fellow, Department of System Dynamics and Control, email: manuel.pusch@dlr.de

outputs. Respective algorithms as summarized, for instance, in Ref. 9 do not necessarily require an iterative procedure but also do not allow an explicit consideration of the controllability and observability of individual modes.

In this paper, a novel approach is presented for the joint design of input and output blending vectors which maximize the controllability and observability of a single mode in terms of the $\mathcal{H}_2$ norm. Taking into account also an explicit decoupling of modes, independent SISO controllers can then be designed for each mode to be controlled. The proposed modal control approach is described in Section II, where a special focus is put on the scaling of inputs and outputs. For the joint computation of the interdependent input and output blending vectors, an unconstrained optimization problem in a single variable is derived in Section III which can be solved efficiently. Eventually, the effectiveness of the proposed approach is demonstrated by designing a gust load alleviation (GLA) controller for large flexible transport aircraft in Section IV.

II. Modal Control

In this section, the general concept of using virtual inputs and outputs for modal control is presented. The proposed approach allows controlling individual modes by means of SISO controllers independent of the number of inputs, outputs or states of the underlying dynamic system.

A. Modal Decomposition

A linear time-invariant (LTI) system with n_u inputs, n_y outputs and n_x states can be described by the transfer function matrix

$$\boldsymbol{G}(s) = \boldsymbol{C}\left(s\boldsymbol{I} - \boldsymbol{A}\right)^{-1}\boldsymbol{B} + \boldsymbol{D}, \tag{1}$$

where $\boldsymbol{A} \in \mathbb{R}^{n_x \times n_x}, \boldsymbol{B} \in \mathbb{R}^{n_x \times n_u}, \boldsymbol{C} \in \mathbb{R}^{n_y \times n_x}, \boldsymbol{D} \in \mathbb{R}^{n_y \times n_u}$ and s denoting the Laplace variable. Assuming that $\boldsymbol{A}$ is diagonalizable, a modal decomposition of $\boldsymbol{G}(s)$ is possible such that

$$\boldsymbol{G}(s) = \sum_{i=1}^{n_i} \boldsymbol{M}_i(s) + \boldsymbol{D}, \tag{2}$$

where the individual modes $i = 1, ..., n_i$ are given as

$$\boldsymbol{M}_i(s) = \begin{cases} \dfrac{\boldsymbol{R}_{p_i}}{s - p_i} & \text{if } \Im(p_i) = 0 \\ \dfrac{\boldsymbol{R}_{p_i}}{s - p_i} + \dfrac{\overline{\boldsymbol{R}}_{p_i}}{s - \overline{p}_i} & \text{otherwise.} \end{cases} \tag{3}$$

According to Equation (3), a mode i is either described by a single real pole p_i with an imaginary part $\Im(p_i) = 0$ or a conjugate complex pole pair p_i and $\overline{p}_i$. Hence, the number of modes n_i does not necessarily equal the number of states n_x as conjugate complex pole pairs are considered as single modes. Each pole p_i is associated with a residue $\boldsymbol{R}_{p_i} = \boldsymbol{c}_{p_i}^T \boldsymbol{b}_{p_i} \in \mathbb{C}^{n_y \times n_u}$, where $\boldsymbol{b}_{p_i} \in \mathbb{C}^{n_u}$ and $\boldsymbol{c}_{p_i} \in \mathbb{C}^{n_y}$ are the pole input and output vectors, respectively. For a real pole, the corresponding pole vectors and residue are also real and for a conjugate complex pole pair the pole vectors and residues are also conjugate complex.

Furthermore, the natural frequency of a mode is given as

$$\omega_\mathrm{n} = |p_i| \tag{4}$$

and for $\omega_\mathrm{n} \neq 0$, the corresponding relative damping is

$$\zeta = -\Re(p_i)/\omega_\mathrm{n}. \tag{5}$$

Note that for a conjugate complex pole pair, the corresponding real parts $\Re(p_i) = \Re(\overline{p}_i)$ and magnitudes $|p_i| = |\overline{p}_i|$ are equal. For more information on modal decomposition and the properties of individual modes see, for instance, Ref. 5.

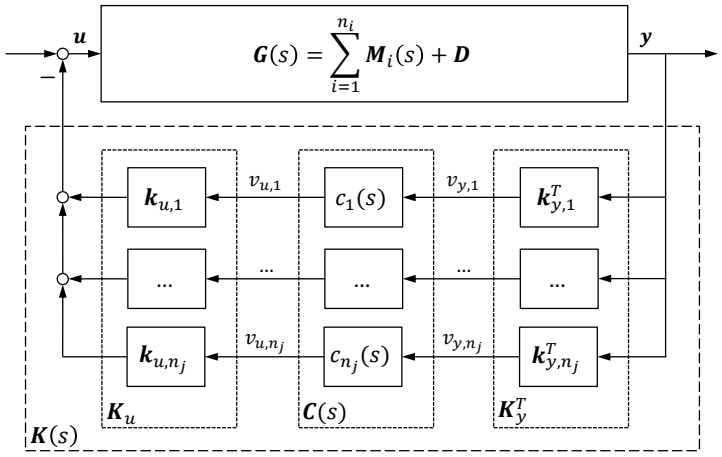

Figure 1: Closed-loop interconnection of the plant $G(s)$ with the controller $K(s)$

B. Modal Control using Virtual Inputs and Outputs

The task of controlling a single mode of a high order dynamic system $\boldsymbol{G}(s)$ can quickly become challenging when the number of control inputs or measurement outputs is increased. In order to reduce the complexity of the control problem, it is proposed to generate a virtual control input $v_{u,j}$ and a virtual measurement output $v_{y,j}$ to isolate the modes $\boldsymbol{M}_j(s), j = 1, .., n_j$ to be controlled, where $\{\boldsymbol{M}_j(s)\} \subseteq \{\boldsymbol{M}_i(s)\}$. To that end, the input and output signals of the plant are blended using the blending vectors $\boldsymbol{k}_{u,j} \in \mathbb{R}^{n_u}$ and $\boldsymbol{k}_{y,j} \in \mathbb{R}^{n_y}$. This allows a decoupling of modes which enables to design SISO controllers $c_j(s)$ for each mode to be controlled. Furthermore, the blending vectors can be seen as directional filters depending rather on the shape but not frequency of the targeted mode and thus, a great robustness against frequency variations can be achieved.

The resulting feedback interconnection is depicted in Figure 1, where the controller

$$\boldsymbol{K}(s) = \boldsymbol{K}_u \boldsymbol{C}(s) \boldsymbol{K}_y^T, \tag{6}$$

with the SISO controllers listed on the diagonal of

$$\boldsymbol{C}(s) = \operatorname{diag}\left(c_1(s), \cdots, c_{n_j}(s)\right) \tag{7}$$

and the blending vectors summarized in

$$\boldsymbol{K}_u = \begin{bmatrix} \boldsymbol{k}_{u,1} & \cdots & \boldsymbol{k}_{u,n_j} \end{bmatrix} \tag{8}$$

$$\boldsymbol{K}_y = \begin{bmatrix} \boldsymbol{k}_{y,1} & \cdots & \boldsymbol{k}_{y,n_j} \end{bmatrix}. \tag{9}$$

C. Scaling

For a proper blending vector design, an appropriate scaling is crucial as different signals with possibly different physical units are united in a single one. To that end, it has to be distinguished between the scaling of the plant's inputs and outputs and the scaling of the virtual inputs and outputs generated for modal control. For the plant inputs and outputs, it is proposed to group the respective signals according to their physical unit and to scale them in groups. This allows for normalizing different physical units among each other while maintaining the relative importance of individual signals. For the virtual input and output signals, a normalization of the magnitudes is recommended in order to support the subsequent SISO controller design.

Considering the proposed scalings, the blending vectors defined in Section II.B can be split up into

$$\boldsymbol{k}_{u,j} = \boldsymbol{\Lambda}_u \boldsymbol{k}_{u,j}^* \lambda_{u,j} \tag{10}$$

$$\boldsymbol{k}_{y,j} = \boldsymbol{\Lambda}_y \boldsymbol{k}_{y,j}^* \lambda_{y,j}\ , \tag{11}$$

where the diagonal matrices $\boldsymbol{\Lambda}_u \in \mathbb{R}^{n_u \times n_u}$ and $\boldsymbol{\Lambda}_y \in \mathbb{R}^{n_y \times n_y}$ scale the inputs and outputs of the plant and the scaling factors $\lambda_{u,j} \in \mathbb{R}$ and $\lambda_{y,j} \in \mathbb{R}$ are introduced to normalize the virtual input and output signals. The actual optimal input and output blending vectors $\boldsymbol{k}_{u,j}^* \in \mathbb{R}^{n_u}$ and $\boldsymbol{k}_{y,j}^* \in \mathbb{R}^{n_y}$ are considered to be of unit length and derived in Section III.

D. Summary of the Proposed Controller Design Procedure

The proposed controller design procedure for modal control can be divided into three main parts as depicted in Figure 2. First, a modal decomposition is carried out and the modes to be controlled are selected. Second, input and output blending vectors are designed for each selected mode and, as a result, dedicated virtual inputs and outputs are generated. Note that for a proper blending vector design, it is proposed to scale all inputs and outputs as described in the previous section. Finally, SISO controllers are designed for each mode to be controlled, where the individual controllers may be designed simultaneously or in a sequential way. For the latter, each SISO loop is closed before the next SISO controller is designed. Note that due to a limited number of control inputs and measurement outputs, a perfect mode decoupling may not always be possible. In that case, the modal decomposition may be repeated after closing a SISO loop which is indicated by the dashed arrow in Figure 2.

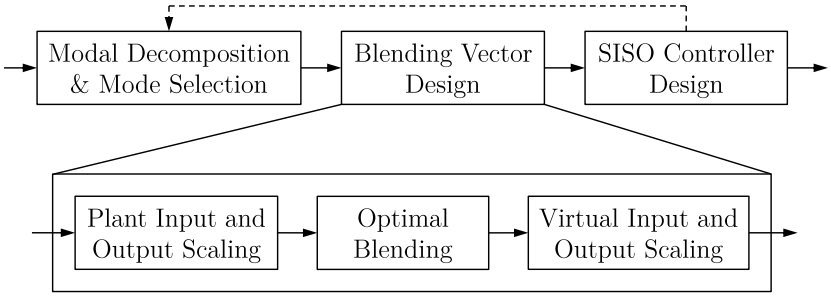

Figure 2: Proposed Controller Design Procedure

III. Optimal Blending of Inputs and Outputs for Modal Control

For the design of the input and output blending vectors, two main objectives are considered in this paper. On the one hand, a sufficient mode decoupling has to be achieved in order to enable the proposed SISO controller design. On the other hand, a maximum controllability and observability of the targeted mode is desired. As controllability and observability can not be regarded independent of each other, a joint design of the respective input and output blending vectors is required. In the following, an appropriate optimization problem is formulated and a procedure for solving it is derived.

A. Problem Statement

In this paper, the combined controllability and observability of an asymptotically stable mode $\boldsymbol{M}(s) \in \{\boldsymbol{M}_j(s)\}$ is quantified in terms of the $\mathcal{H}_2$ norm. By blending control inputs and measurement outputs with real-valued unit vectors $\boldsymbol{k}_u$ and $\boldsymbol{k}_y$, this measure can not be increased but is rather decreased. This loss of controllability and observability can be quantified by the efficiency factor

$$\eta = \frac{\left\|\boldsymbol{k}_y^T \boldsymbol{M}(s) \boldsymbol{k}_u\right\|_{\mathcal{H}_2}}{\left\|\boldsymbol{M}(s)\right\|_{\mathcal{H}_2}}, \tag{12}$$

where $\eta \in [0\ 1]$ when $\left\|\boldsymbol{M}(s)\right\|_{\mathcal{H}_2}$ is finite, which is the case since $\boldsymbol{M}(s)$ is assumed to be asymptotically stable and strictly proper. Based on that, a pair of input and output blending vectors is considered as $\mathcal{H}_2$-optimal when the efficiency factor η is maximized. The resulting optimization problem can hence be formulated as

$$\begin{aligned} \underset{\boldsymbol{k}_u \in \mathbb{R}^{n_u}, \boldsymbol{k}_y \in \mathbb{R}^{n_y}}{\text{maximize}} \quad & \left\|\boldsymbol{k}_y^T \boldsymbol{M}(s) \boldsymbol{k}_u\right\|_{\mathcal{H}_2} \\ \text{subject to} \quad & \left\|\boldsymbol{k}_u\right\|_2 = 1 \\ & \left\|\boldsymbol{k}_y\right\|_2 = 1. \end{aligned} \tag{13}$$

In the following Section III.B, preliminaries are described which support the derivation of an efficient solution procedure for (13) given in Section III.C. In order to consider also the desired mode decoupling, additional optimization constraints are proposed in Section III.D and eventually, a solution of the overall optimization problem is summarized in Section III.E.

B. Preliminaries

1. $\mathcal{H}_2$ norm of a first or second order SISO system

The optimization problem (13) requires to maximize the $\mathcal{H}_2$ norm of the asymptotically stable SISO system

$$m(s) = \boldsymbol{k}_y^T \boldsymbol{M}(s) \boldsymbol{k}_u, \tag{14}$$

which has a maximum order of two. For this special type of LTI system, it can be shown that

$$\|m(s)\|_{\mathcal{H}_2} = |m(i\omega_\mathrm{n})| \sqrt{\zeta \omega_\mathrm{n}}, \tag{15}$$

where ω_n and ζ are the natural frequency and the relative damping of a single mode as defined in Section II.A. Note that in Equation (15), the complex variable $i = \sqrt{-1}$ is not to be confused with the subscript i defined in Section II.A to index individual modes. As the term $\sqrt{\zeta \omega_\mathrm{n}}$ in Equation (15) is independent of the actual blending vectors, the original problem of maximizing the $\mathcal{H}_2$ norm in (13) can be turned into a problem of maximizing the magnitude of the complex scalar $z = m(i\omega_\mathrm{n})$.

2. Magnitude of a complex scalar

The magnitude of a complex scalar $z \neq 0$ with a phase angle $\phi^* = \arg z$ can be computed by rotating z onto the positive real axis in the complex plane. As it is illustrated in Figure 3, the clockwise rotation of z by an angle $\phi \in \mathbb{R}$, described as

$$\begin{aligned} \tilde{z}(\phi) &= \big(\Re(z) + i\Im(z)\big)\,(\cos\phi - i\sin\phi) \\ &= \underbrace{\Re(z)\cos\phi + \Im(z)\sin\phi}_{\Re(\tilde{z}(\phi))} + i\,\underbrace{\big(\Im(z)\cos\phi - \Re(z)\sin\phi\big)}_{\Im(\tilde{z}(\phi))}, \end{aligned} \tag{16}$$

which results in $\Re(\tilde{z}) = |z|$ and $\Im(\tilde{z}) = 0$ iff $\phi = \phi^*$. Based on that, the magnitude of z can be computed by

$$|z| = \max_\phi \Re\big(\tilde{z}(\phi)\big) = \max_\phi \big(\Re(z)\cos\phi + \Im(z)\sin\phi\big), \tag{17}$$

where the real part of $\tilde{z}(\phi)$ is maximized for $\phi = \phi^*$.

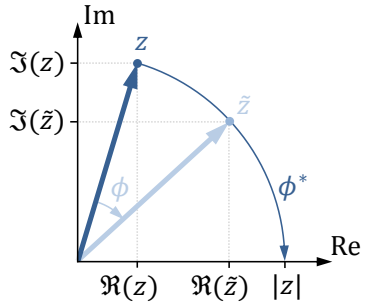

Figure 3: Determination of the magnitude of the complex scalar z by rotating it onto the positive real axis.

C. Computation of $\mathcal{H}_2$-optimal Blending Vectors

In the following, an equivalent to the optimization problem (13) is derived which allows for an efficient computation of the $\mathcal{H}_2$-optimal blending vectors by taking into account the preliminaries of Section III.B.

To begin with, Equation (17) is taken and $z = \boldsymbol{k}_y^T \boldsymbol{M}(j\omega_\mathrm{n})\boldsymbol{k}_u$ is inserted. Factoring out the real-valued blending vectors $\boldsymbol{k}_y$ and $\boldsymbol{k}_u$ leads to

$$\begin{aligned} |\boldsymbol{k}_y^T \boldsymbol{M}(j\omega_\mathrm{n})\boldsymbol{k}_u| &= \max_\phi \big(\boldsymbol{k}_y^T \big(\Re(\boldsymbol{M}(j\omega_\mathrm{n}))\cos\phi + \Im(\boldsymbol{M}(j\omega_\mathrm{n}))\sin\phi\big)\boldsymbol{k}_u\big) \\ &= \max_\phi \big(\boldsymbol{k}_y^T \boldsymbol{F}(\phi)\boldsymbol{k}_u\big), \end{aligned} \tag{18}$$

where $\boldsymbol{F}(\phi) : \mathbb{R} \to \mathbb{R}^{n_y \times n_u}$ is defined as

$$\boldsymbol{F}(\phi) = \Re(\boldsymbol{M}(j\omega_\mathrm{n}))\cos\phi + \Im(\boldsymbol{M}(j\omega_\mathrm{n}))\sin\phi. \tag{19}$$

Recalling that the actual goal is to find a maximum of Equation (18) gives

$$\begin{aligned}\max_{\boldsymbol{k}_u,\boldsymbol{k}_y} \left|\boldsymbol{k}_y^T \boldsymbol{M}(j\omega_\mathrm{n})\boldsymbol{k}_u\right| &= \max_{\boldsymbol{k}_u,\boldsymbol{k}_y} \max_{\phi} \left(\boldsymbol{k}_y^T \boldsymbol{F}(\phi)\boldsymbol{k}_u\right) \\ &= \max_{\phi} \max_{\boldsymbol{k}_u,\boldsymbol{k}_y} \left(\boldsymbol{k}_y^T \boldsymbol{F}(\phi)\boldsymbol{k}_u\right).\end{aligned} \tag{20}$$

In Equation (20), the term

$$\max_{\boldsymbol{k}_u,\boldsymbol{k}_y} \left(\boldsymbol{k}_y^T \boldsymbol{F}(\phi)\boldsymbol{k}_u\right) = \left\|\boldsymbol{F}(\phi)\right\|_2 = \sigma_\mathrm{max} \tag{21}$$

can be directly computed for a given value of ϕ by applying a singular value decomposition (SVD) on

$$\boldsymbol{F}(\phi) = \boldsymbol{U}\boldsymbol{\Sigma}\boldsymbol{V}^T = \begin{bmatrix}\boldsymbol{k}_{y,\mathrm{max}} & \bullet\end{bmatrix} \begin{bmatrix}\sigma_\mathrm{max} & \boldsymbol{0} \\ \boldsymbol{0} & \bullet\end{bmatrix} \begin{bmatrix}\boldsymbol{k}_{u,\mathrm{max}} & \bullet\end{bmatrix}^T, \tag{22}$$

where the placeholder $\bullet$ denotes a matrix of adequate size. In Equation (22), both $\boldsymbol{U} \in \mathbb{R}^{n_y \times n_y}$ and $\boldsymbol{V} \in \mathbb{R}^{n_u \times n_u}$ are orthogonal matrices which are real-valued as $\boldsymbol{F}(\phi)$ is also real-valued. Furthermore, $\boldsymbol{\Sigma} \in \mathbb{R}^{n_y \times n_u}$ is a rectangular diagonal matrix with the singular values of $\boldsymbol{F}(\phi)$ in descending order on its diagonal. Selecting only the largest singular value $\sigma_\mathrm{max} \in \mathbb{R}_{\geq 0}$, the corresponding input and output singular vectors $\boldsymbol{k}_{u,\mathrm{max}} \in \mathbb{R}^{n_u}$ and $\boldsymbol{k}_{y,\mathrm{max}} \in \mathbb{R}^{n_y}$ directly yield the input and output blending vectors which solve Equation (21) for a given value of ϕ.

Finally, inserting Equation (21) into Equation (20), an equivalent to optimization problem (13) can be derived as

$$\max_{\boldsymbol{k}_u,\boldsymbol{k}_y} \left\|\boldsymbol{k}_y^T \boldsymbol{M}(s)\boldsymbol{k}_u\right\|_{\mathcal{H}_2} \Leftrightarrow \max_{\phi} \left\|\boldsymbol{F}(\phi)\right\|_2, \tag{23}$$

where $\boldsymbol{k}_u \in \mathbb{R}^{n_u}$ and $\boldsymbol{k}_y \in \mathbb{R}^{n_y}$ are constrained by $\left\|\boldsymbol{k}_u\right\|_2 = 1$ and $\left\|\boldsymbol{k}_y\right\|_2 = 1$ while $\phi \in \mathbb{R}$ is unconstrained. Solving the unconstrained optimization problem in Equation (23) yields an optimal phase angle for which the $\mathcal{H}_2$-optimal blending vectors can be directly determined according to Equation (22). Hence, the number of optimization variables is reduced from $n_u + n_y$ to a single one, or, in other words, the difficulty of finding a solution of (13) becomes independent of the actual number of inputs and outputs.

D. Mode Decoupling

So far, $\mathcal{H}_2$-optimal blending vectors are derived which maximize the controllability and observability of the targeted mode. For mode decoupling, however, it is additionally desired that the resulting virtual inputs and outputs prevent an excitation or measurement of certain residual modes. This can be achieved by enforcing the input and output blending vectors to be orthogonal on the pole input and output vectors of the respective residual modes. For a complex-valued pole vector, this means that orthogonality is enforced on both the real and imaginary part as the blending vectors are real-valued. Collecting the real and imaginary parts of the respective pole input and output vectors as row vectors in the matrices $\boldsymbol{Q}_u$ and $\boldsymbol{Q}_y$, the original optimization problem (13) can be augmented as

$$\begin{aligned}\underset{\boldsymbol{k}_u \in \mathbb{R}^{n_u}, \boldsymbol{k}_y \in \mathbb{R}^{n_y}}{\text{maximize}} \quad & \left\|\boldsymbol{k}_y^T \boldsymbol{M}(s)\boldsymbol{k}_u\right\|_{\mathcal{H}_2} \\ \text{subject to} \quad & \left\|\boldsymbol{k}_u\right\|_2 = 1 \\ & \left\|\boldsymbol{k}_y\right\|_2 = 1 \\ & \boldsymbol{Q}_u\boldsymbol{k}_u = 0 \\ & \boldsymbol{Q}_y\boldsymbol{k}_y = 0,\end{aligned} \tag{24}$$

where the constraints $\boldsymbol{Q}_u\boldsymbol{k}_u = 0$ and $\boldsymbol{Q}_y\boldsymbol{k}_y = 0$ enforce the desired mode decoupling. For the blending vectors $\boldsymbol{k}_u$ and $\boldsymbol{k}_y$, this means that they are restricted to the null space of $\boldsymbol{Q}_u$ and $\boldsymbol{Q}_y$. If one of the null spaces is

empty, meaning that $\boldsymbol{Q}_u$ or $\boldsymbol{Q}_y$ has full rank, the augmented optimization problem (24) is infeasible. This also implies that for a finite number of inputs and outputs, the number of residual modes which can be made uncontrollable or unobservable is limited. Note, however, that for mode decoupling it may be sufficient to make the respective residual modes either uncontrollable or unobservable but not both.

In order to solve the augmented optimization problem (24), the original optimization variables $\boldsymbol{k}_u$ and $\boldsymbol{k}_y$ are substituted by

$$\boldsymbol{k}_u = \boldsymbol{N}_u \tilde{\boldsymbol{k}}_u \tag{25}$$

$$\boldsymbol{k}_y = \boldsymbol{N}_y \tilde{\boldsymbol{k}}_y \ , \tag{26}$$

where $\boldsymbol{N}_u$ and $\boldsymbol{N}_y$ denote an orthonormal basis of the null space of $\boldsymbol{Q}_u$ and $\boldsymbol{Q}_y$, respectively. With the vectors $\tilde{\boldsymbol{k}}_u$ and $\tilde{\boldsymbol{k}}_y$ as new optimization variables, the equivalent optimization problem (23) can be turned into

$$\max_{\tilde{\boldsymbol{k}}_u, \tilde{\boldsymbol{k}}_y} \left\| \tilde{\boldsymbol{k}}_y^T \boldsymbol{N}_y^T \boldsymbol{M}_j(s) \boldsymbol{N}_u \tilde{\boldsymbol{k}}_u \right\|_{\mathcal{H}_2} \quad \Leftrightarrow \quad \max_{\phi} \left\| \boldsymbol{N}_y^T \boldsymbol{F}(\phi) \boldsymbol{N}_u \right\|_2 , \tag{27}$$

since the real-valued matrices $\boldsymbol{N}_u$ and $\boldsymbol{N}_y$ act as unitary linear transformations preserving the inner product. This means that if $\tilde{\boldsymbol{k}}_u$ and $\tilde{\boldsymbol{k}}_u$ are real-valued unit vectors, $\boldsymbol{k}_u$ and $\boldsymbol{k}_u$ are also real-valued unit vectors. Solving the equivalent optimization problem (27) for ϕ, solutions for $\tilde{\boldsymbol{k}}_u$ and $\tilde{\boldsymbol{k}}_y$ can be determined by the SVD in Equation (22) directly yielding the $\mathcal{H}_2$-optimal blending vectors when multiplied with $\boldsymbol{N}_u$ and $\boldsymbol{N}_y$.

It has to be noted, however, that the additional mode decoupling constraints typically decreases the maximum achievable $\mathcal{H}_2$ norm in the optimization problem (24). Hence, a trade-off between the decoupling of individual modes and the attainable controllability and observability of the mode to be controlled is usually required.

Furthermore, it has to be noted that the described procedure for mode decoupling may also be used to eliminate a non-zero feedthrough matrix $\boldsymbol{D} \neq 0$. For this purpose, the right or left singular vectors of $\boldsymbol{D}$ only need to be added to $\boldsymbol{Q}_u$ or $\boldsymbol{Q}_y$, respectively.

E. Summary of the Proposed Algorithm

Summing up the findings of Section III.C and III.D, the augmented optimization problem (24) including the constraints for mode decoupling can be efficiently solved by first finding an optimal phase angle

$$\phi^* = \arg\max_{\phi \in \mathbb{R}} \left\| \boldsymbol{N}_y^T \boldsymbol{F}(\phi) \boldsymbol{N}_u \right\|_2 , \tag{28}$$

where $\boldsymbol{F}(\phi)$ is defined in Equation (19) and the null spaces $\boldsymbol{N}_u$ and $\boldsymbol{N}_y$ for mode decoupling are defined in Section III.D. Due to the given periodicity of $\boldsymbol{F}(\phi)$, the search for an optimal phase angle may be restricted to an interval of size π, for instance $\phi \in [0, \pi[$. Note that if the pole and hence residue of the underlying mode is real-valued, the optimal blending vectors can be computed without any optimization by carrying out an SVD on the corresponding residue $\boldsymbol{R}_{p_i}$.

After determining the optimal phase angle ϕ^*, the corresponding $\mathcal{H}_2$-optimal input and output blending vectors $\boldsymbol{k}_u^* = \boldsymbol{N}_u \tilde{\boldsymbol{k}}_u^*$ and $\boldsymbol{k}_y^* = \boldsymbol{N}_y \tilde{\boldsymbol{k}}_y^*$ can be derived by means of an SVD of

$$\boldsymbol{F}(\phi^*) = \boldsymbol{U} \boldsymbol{\Sigma} \boldsymbol{V}^T = \begin{bmatrix} \tilde{\boldsymbol{k}}_y^* & \bullet \end{bmatrix} \begin{bmatrix} \sigma_{\max}^* & \boldsymbol{0} \\ \boldsymbol{0} & \bullet \end{bmatrix} \begin{bmatrix} \tilde{\boldsymbol{k}}_u^* & \bullet \end{bmatrix}^T , \tag{29}$$

where $\sigma_{\max}^* = \|\boldsymbol{F}(\phi^*)\|_2 = \left\| \boldsymbol{N}_y^T \boldsymbol{F}(\phi^*) \boldsymbol{N}_u \right\|_2$ is the optimal value of the objective function of Equation (28).

Note that the optimal phase angle and the resulting optimal blending vectors are not necessarily unique. This can be shown at the example when the real and imaginary part of $\boldsymbol{M}(j\omega_\mathrm{n})$ have equal singular values but orthogonal singular vectors.

IV. Application: Gust Load Alleviation

For the evaluation of the effectiveness of the proposed control approach, a GLA system is designed for a flexible aircraft with distributed flaps and measurements. To that end, the nonlinear aeroelastic aircraft model of industrial complexity is linearized and a modal decomposition is carried out. After selecting the aeroelastic modes that should be controlled, corresponding input and output blending vectors are designed, where an explicit decoupling from modes like the short period motion is considered. Subsequently, independent SISO controllers are designed in order to increase the relative damping of the selected aeroelastic modes. Eventually, the performance of the resulting GLA system is evaluated in terms of the reduction of the wing root bending moment (WRBM) during gust encounters.

A. Flexible Aircraft Modeling

The flexible aircraft used in this paper is modeled according to Ref. 10 and is a derivative of the one used in Ref. 11. The aeroelastic model interconnects a finite element model of the airframe with a model of the unsteady aerodynamics. The unsteady aerodynamics model is computed in frequency domain by means of the doublet lattice method[12] and transformed to time domain using Roger's rational function approximation.[13] For the gust input, the aircraft is divided into 30 zones in the direction of flight and a Padé approximation is used to model the time delay for each zone. As control surfaces, a pair of elevators and 9 equally distributed trailing edge flaps on each wing are modeled as illustrated in Figure 4. The actuators for each control surface are approximated by a second order Butterworth low pass filter with a cutoff frequency of $\omega_c = 40\,\mathrm{rad/s}$. Eventually, the resulting structural loads are recovered by the force summation method described in Ref. 6. For more details on aeroelastic modeling see also Refs. 10, 12, 14.

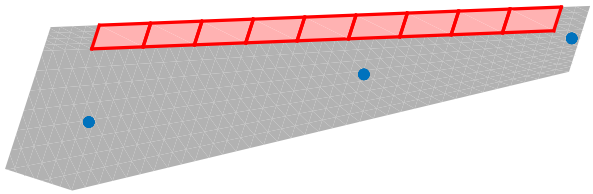

Figure 4: Distributed trailing edge flaps (red) and sensor locations (blue) on the wing.

The response of the flexible aircraft is captured by 11 distributed inertial measurement units (IMUs), where 2 IMUs are placed on the tips of the horizontal tail plane (HTP), 3 IMUs are placed on each wing and 3 IMUs are placed along the fuselage. Each of the IMU measures the rotational rates and translational accelerations in three spatial directions.

Furthermore, only symmetric excitations are taken into account, meaning that the gust encounter, the measurement signals and the control surface deflections are assumed to be equal on the left and right hand side of the aircraft. This allows discarding all non-symmetric structural modes leading to a longitudinal aircraft model with a reduced number of inputs, outputs and states.

For the proposed control approach, the nonlinear aircraft model is linearized around steady horizontal flight at $Ma = 0.86$ and $h = 9108\,\mathrm{m}$, where the phugoid mode is truncated as it is outside the frequency range of interest for GLA. The resulting LTI system is of order 264 and has 1 vertical gust and 10 control surface inputs. As outputs, besides the 66 measurement signals from the distributed IMUs, also the WRBM is computed to evaluate the efficiency of the GLA system.

B. Modal Decomposition and Mode Selection

Taking the LTI model described in the previous section, a modal decomposition is carried out with the aeroelastic modes in the frequency range of interest listed in Table 1. As it is typical for highly flexible aeroelastic systems, all modes besides the short period mode (rigid body) are very lightly damped and the distances between the respective frequencies are small.

In order to allow a systematic selection of the modes to be controlled, their respective dominance needs to be quantified. To that end, $\tilde{\boldsymbol{M}}_i(s)$ is defined as the transfer function of a single mode i from the vertical gust input to the WRBM output, or in general terms, from the disturbance inputs to the performance outputs. Based on that, the dominance of each mode can be quantified by $\left\|\tilde{\boldsymbol{M}}_i(s)\right\|_{\mathcal{H}_2}$, where the $\mathcal{H}_2$ norm is used in

a similar manner as for the evaluation of the combined controllability and observability in Section III.A. For the given aeroelastic modes, the first and second wing bending mode are the most dominant ones according to the last column in Table 1. For the purpose of GLA, it is hence desired to increase the damping of the two modes, where it is worth to mention that the short period mode is already controlled by the flight control system. Note that the respective modal dominances can also be recognized in the open-loop frequency response depicted in Figure 7 in Section IV.E.

Table 1: Symmetric aeroelastic modes in the frequency range of interest

i	mode name	natural frequency $\omega_{\mathrm{n},i}$ (rad/s)	relative damping ζ_i (-)	normalized dominance $\left\|\tilde{\boldsymbol{M}}_i(s)\right\|_{\mathcal{H}_2}$
1	short period	1.6	0.42	0.167
2	first wing bending	10.9	0.12	1.000
3	first wing torsion	15.6	0.03	0.033
4	first engine	18.4	0.03	0.019
5	first wing inplane	21.9	0.03	0.067
6	second wing bending	25.2	0.05	0.175
7	first HTP bending	34.4	0.05	0.038

C. Blending of Inputs and Outputs

As described, the goal of the GLA system is to increase the relative damping of the first and second wing bending mode. In order to maintain handling qualities, however, it is required that the short period mode is not affected by the GLA system. To that end, the input and output blending vectors are designed such that the short period mode is explicitly made unobservable and uncontrollable.

Furthermore, it should be ensured that the wing torsion, the HTP bending and the engine mode listed in Table 1 are not excited while increasing the damping of the two wing bending modes. This means that it is sufficient to either make the three modes uncontrollable by the virtual inputs or unobservable by the virtual outputs. For the latter, the maximum achievable $\mathcal{H}_2$ norm (13) is considerably larger because the number of available measurements is much larger than the number of available control surfaces. For this reason, the three modes are only made unobservable by the virtual outputs, degrading the combined controllability and observability of the first and second wing bending mode only slightly. Note that the wing inplane mode at 21.9 rad/s is not taken into account during blending vector design as its controllability and observability is small anyways.

To allow for an independent SISO controller design for the two wing bending modes, the corresponding virtual inputs and outputs also need to be decoupled. For this purpose, the input and output blending vectors associated to one mode are enforced to be orthogonal on the input and output pole vectors of the other mode and vice versa.

The overall achieved decoupling can be reviewed by the frequency response depicted in Figure 5. It can be seen that the virtual input of one mode is hardly measurable by the virtual output of the other mode, which is actually required for an independent SISO controller design. The peaks at the natural frequencies of the first and second wing bending mode indicate a good controllability and observability of the respective modes while the contribution of other nearby modes is negligibly small. In addition to that, the achieved decoupling can also be examined in terms of invariant zeros placed at the location of the poles which should not be excited as it is illustrated in Figure 6 in Section IV.E.

D. SISO Controller Design

After blending inputs and outputs, independent proportional integral (PI) controllers are designed for the first and second wing bending mode. The respective gains are tuned by hand with the goal to minimize the WRBM during gust encounter while satisfying actuator limitations and robustness requirements. For the gust encounter, both are considered a discrete "1-cos" gust excitation and a stochastic gust excitation based on a Dryden filter. The control surface deflections are limited by $\pm 20°$ and the deflection rates are limited by $\pm 60\,°/\mathrm{s}$. In order to achieve the desired robustness, classical gain and phase margins of at least 6 dB and 45°

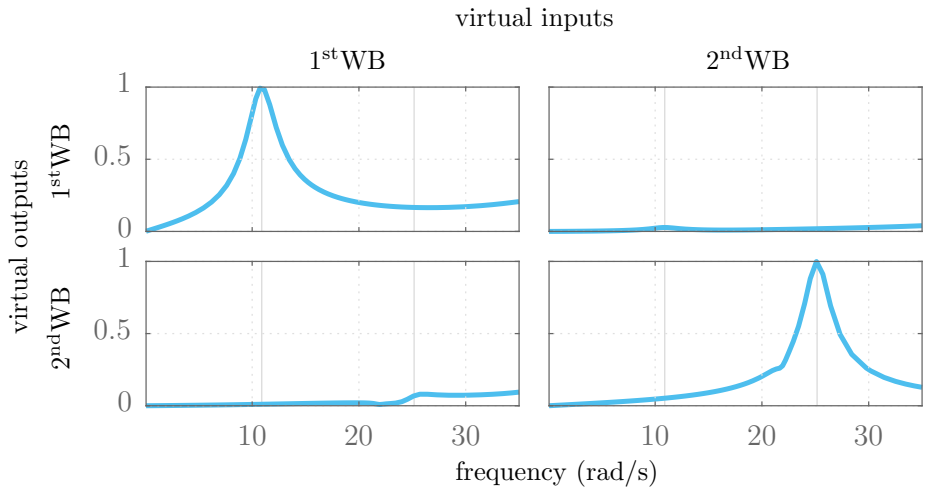

Figure 5: Normalized frequency response from virtual inputs to virtual outputs to control the first and second wing bending mode 1st WB and 2nd WB.

are required, where the individual loops are cut open at the virtual as well as real inputs and outputs of the underlying system.

E. Results

Closing the individual SISO loops, the poles of the aeroelastic system are shifted as depicted in Figure 6. It can be seen that the relative damping of the first and second wing bending mode is increased by a factor of more than 2.5 while the other poles are not or only marginally displaced. The effect of increasing the modal damping on the WRBM is illustrated by the frequency response depicted in Figure 7, where the low frequency range covering the short period mode is hardly affected by the GLA system. Considering a stochastic gust excitation modeled by a Dryden filter,[15] the expected mean value of the resulting WRBM is reduced by 17 %. For the critical discrete gust excitation,[16,17] the peaks of the WRBM are even reduced by 23 % and additionally, undesired oscillations are effectively suppressed as depicted in Figure 8a. At the same time, the rigid body motions are hardly affected as it can be seen in Figure 8b and Figure 8c. Hence, the proposed control design procedure based on blending of inputs and outputs provides a great potential for the control of aeroelastic systems.

V. Conclusions

In order to facilitate the control design for individual aeroelastic modes, a new approach for blending control inputs and measurement outputs is presented in this paper. To that end, the $\mathcal{H}_2$ norm is introduced as a joint measure of the controllability and observability of a single mode subject to be maximized. The resulting optimization problem is augmented by constraints for mode decoupling, where the required trade-off can be adjusted by the control designer. An efficient algorithm is derived which allows the joint computation of the interdependent input and output blending vectors by solving an unconstrained optimization problem in a single variable.

The effectiveness of the proposed algorithm is evaluated by designing a GLA system for a flexible aircraft with distributed flaps and measurements. To that end, the aeroelastic modes which have the highest impact on the structural loads, represented by the WRBM, are identified in a systematic way. Subsequently, dedicated virtual inputs and outputs are generated using the proposed blending approach, where an excellent decoupling from rigid body motions is achieved. Furthermore, the low frequency modes of the engine, the wing torsion and the HTP bending are explicitly made unobservable in order to avoid an undesired excitation. By designing a simple PI controller for each selected aeroelastic mode, the respective damping is increased leading to reduction of the maximum WRBM of 23 % for the critical gust excitation.

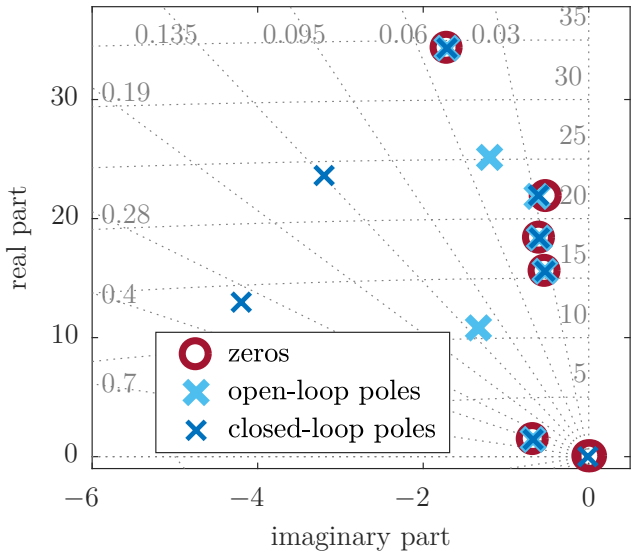

Figure 6: Poles and zeros of the open-loop and closed-loop longitudinal aircraft model with blended inputs and outputs.

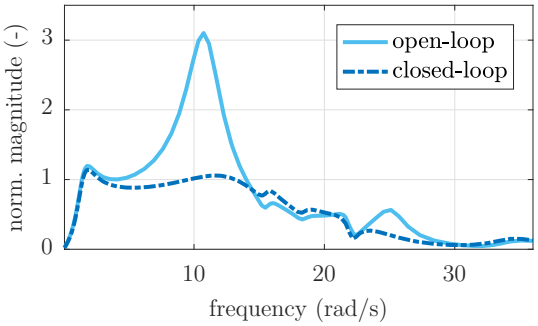

Figure 7: Comparison of frequency response from vertical gust to wing root bending moment.

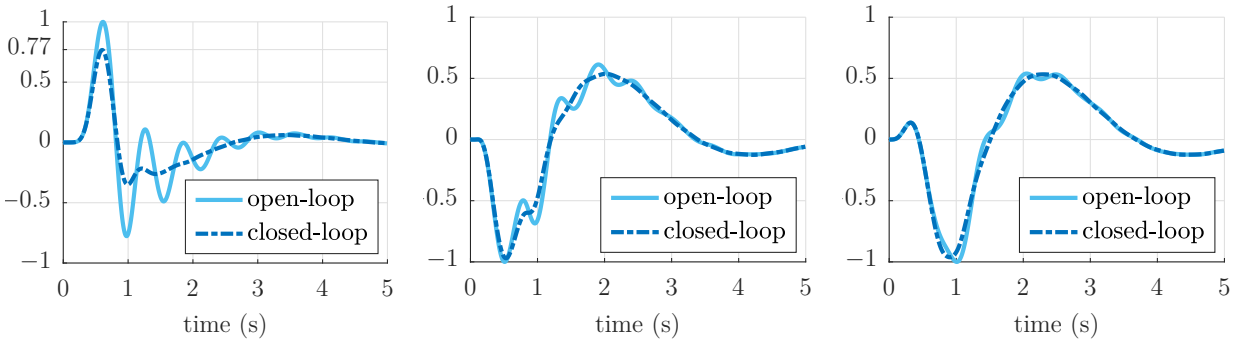

(a) WRBM **(b) vertical acceleration** **(c) pitch rate**

Figure 8: Time responses for critical discrete gust excitation (normalized)

VI. Acknowledgment

The author thanks Wim van Ekeren, Thiemo Kier, Daniel Ossmann and Julian Theis for their insights and helpful discussions. This work was founded in the frame of the German Aeronautical Research Program project "Atlas^{2}Hybrid", grant number 20A1303B.

References

[1]International Energy Agency. *Transport, Energy and CO_2*, 2009.

[2]Christopher D. Regan and Christine V. Jutte. Survey of applications of active control technology for gust alleviation and new challenges for lighter-weight aircraft. Technical Report NASA/TM-2012-216008, NASA, 2012.

[3]Daniel Reckzeh. Multifunctional wing moveables design of the A350XWB and the way to future concepts. In *29th Congress of the International Council of the Aeronautical Sciences (ICAS), St. Petersburg*, 2014.

[4]Andras Varga. Computational challenges in flight control design. In *IEEE International Symposium on computer Aided control System Design, Hawaii, USA*, pages 1–6, 1999.

[5]Sigurd Skogestad and Ian Postlethwaite. *Multivariable feedback control: analysis and design*, volume 2. Wiley New York, 2007.

[6]R. Bisplinghoff, H. Ashley, and R. Halfman. Aeroelasticity, 1955.

[7]Brian P. Danowsky, Peter Thompson, Dong-Chan Lee, and Martin J. Brenner. Modal isolation and damping for adaptive aeroservoelastic suppression. In *AIAA Atmospheric Flight Mechanics (AFM) Conference, Boston, MA*, 2013.

[8]R. Hoogendijk, M. F. Heertjes, M. J. G. Van de Molengraft, and M. Steinbuch. Directional notch filters for motion control of flexible structures. *Mechatronics*, 24(6):632–639, 2014.

[9]David Vaes. Optimal static decoupling for multivariable control design. *Katholieke Universiteit Leuven, Department of Mechanical Engineering*, 2005.

[10]Thiemo Kier. An integrated loads analysis model including unsteady aerodynamic effects for position and attitude dependent gust fields. In *International Forum on Aeroelasticity and Structural Dynamics*, 2011.

[11]Manuel Pusch. Allocation of distributed flaps for gust load alleviation. In *Control Technology and Applications (CCTA), 2017 IEEE Conference on*, pages 2120–2125. IEEE, 2017.

[12]W.P. Rodden and E.H. Johnson. *MSC.Nastran Version 68, Aeroelastic Analysis and User's Guide*, 2004.

[13]Kenneth L. Roger. Airplane math modelling methods for active control design. *Structures and Materials Panel*, 1977.

[14]Frederic M. Hoblit. *Gust loads on aircraft: concepts and applications*. AIAA, 1988.

[15]Military Standard. Flying qualities of piloted vehicles. Technical report, MIL-STD-1797A, 1990.

[16]European Aviation Safety Agency. *Certification Specifications and Acceptable Means of Compliance for Large Aeroplanes, CS-25, Amendment 16*, 2015.

[17]Federal Aviation Administration. *Federal Aviation Regulations Part 25, Airworthiness Standards: Transport Category*, 2015.